eLIFE elifesciences.org

RESEARCH ARTICLE

Figures and figure supplements

ICE1 promotes the link between splicing and nonsense-mediated mRNA decay

Thomas D Baird *et al*

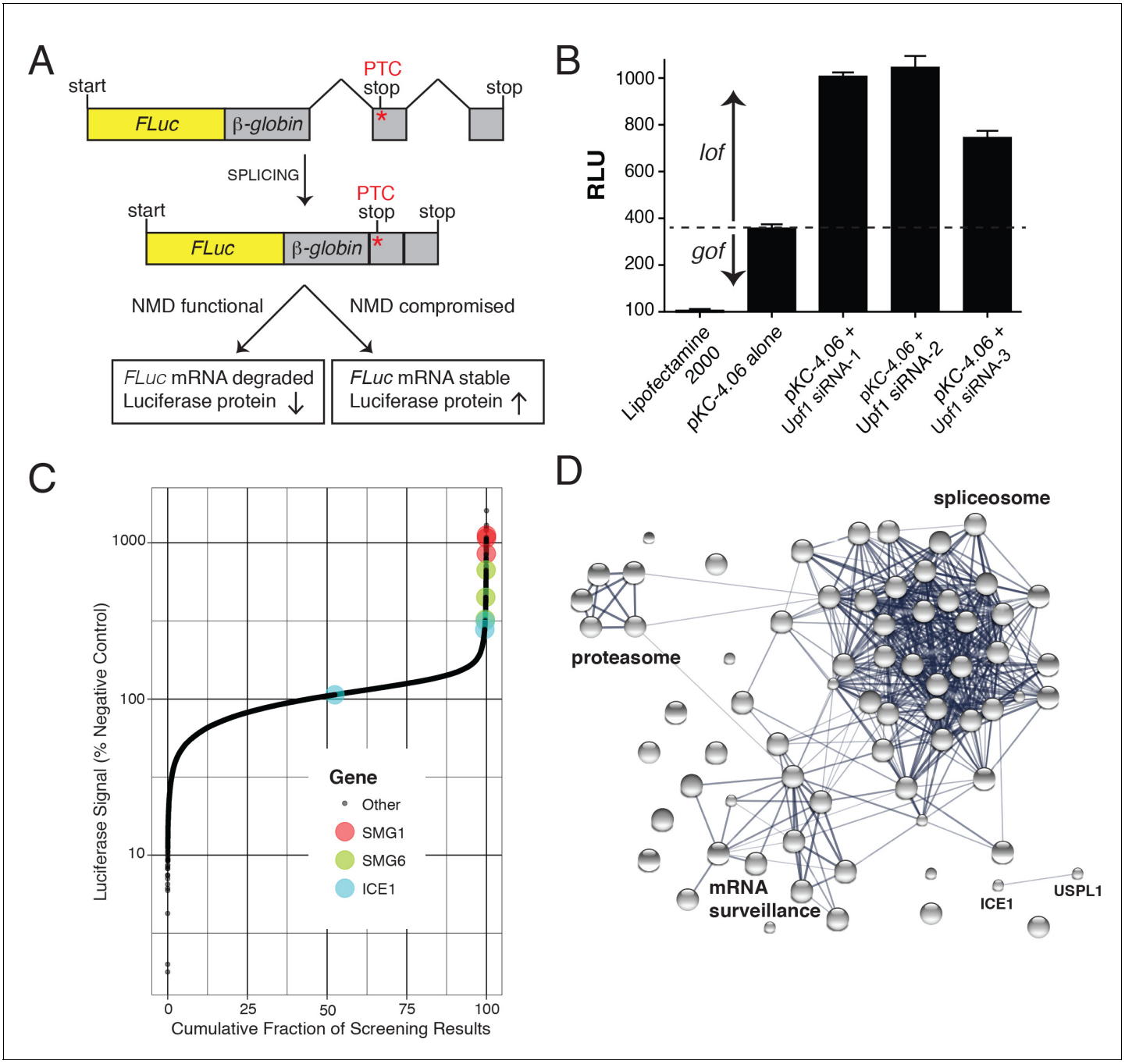

Figure 1. FLuc NMD-targeted assay for high-throughput RNAi screening. (**A**) Fusion construct design of the NMD loss-of-function (lof) gain-of-signal (gos) reporter system (3XFLAG-FLuc-βglobinUGA) where a premature termination codon (PTC) within the second exon of the β-globin gene targets the mRNA for rapid NMD (FLuc, firefly luciferase). (**B**) Silencing of the NMD factor UPF1 using three different siRNAs increased expression of transiently expressed luciferase from the NMD 3XFLAG-FLuc-βglobinUGA construct. (**C**) Control normalized, log-transformed MAD Z-scores of genome-wide siRNA screen illustrating high-ranking genes from the NMD pathway. (**D**) STRING pathway analysis illustrating tight connectivity of highest ranking genes into RNA-associated processing pathways.

DOI: https://doi.org/10.7554/eLife.33178.003

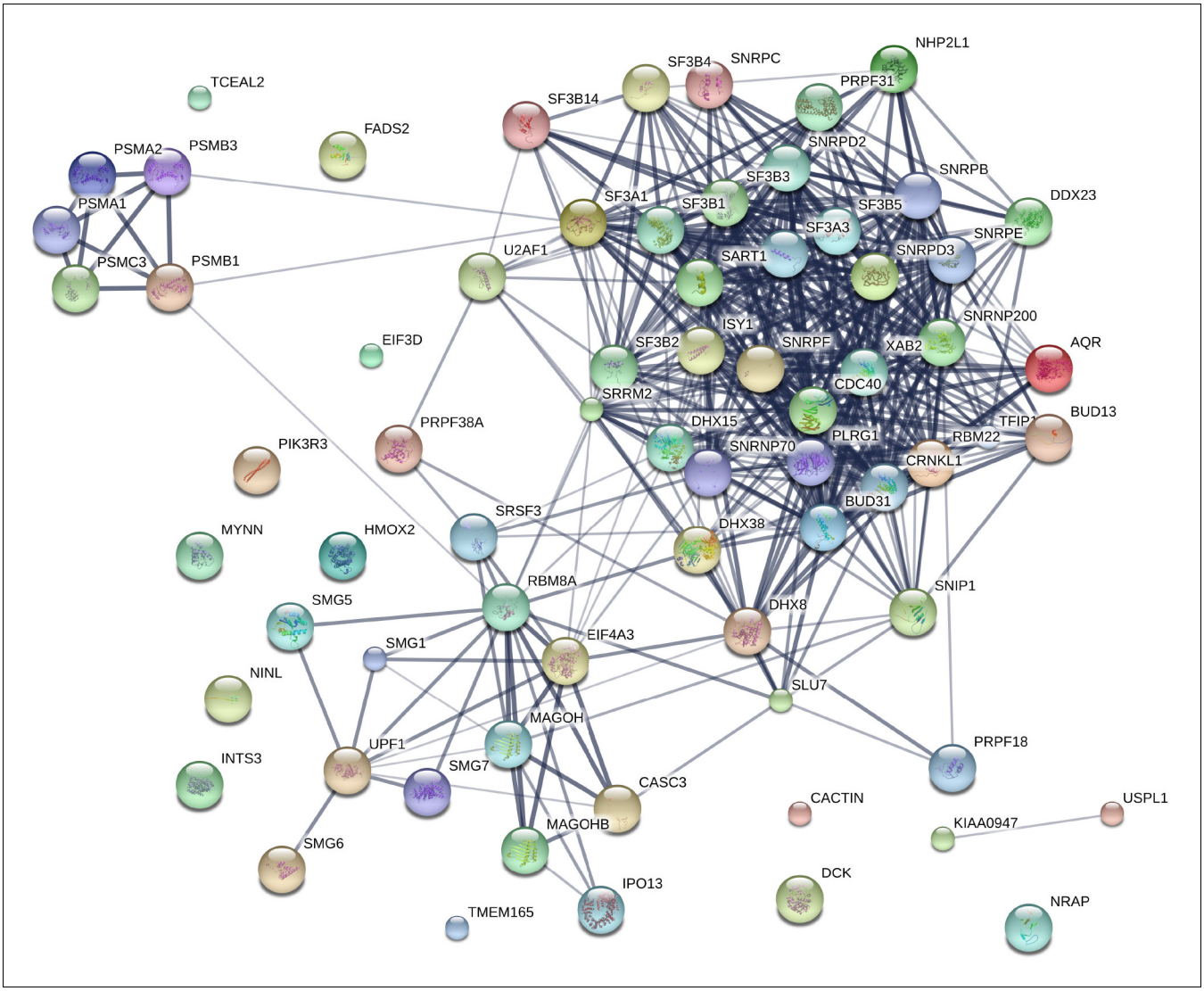

Figure 1—figure supplement 1. STRING network analysis of genes identified in RNAi screen. STRING was used to identify any known interactions between the top screen hits (median seed corrected Z > 1.5). This analysis indicated a significant enrichment in known interactions, including many associated with NMD and the spliceosome.

DOI: https://doi.org/10.7554/eLife.33178.004

A

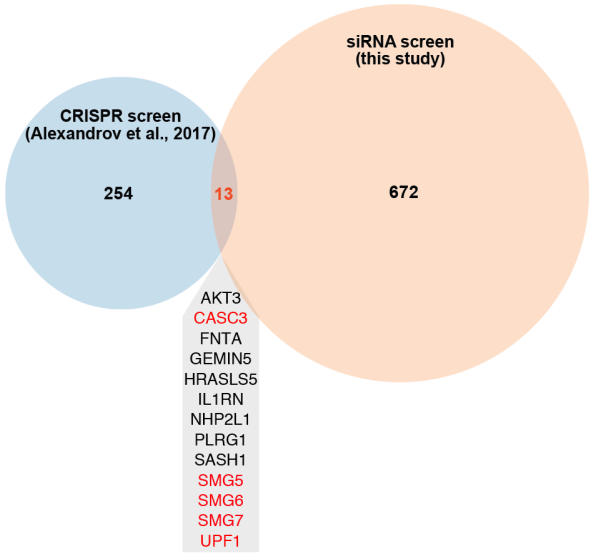

B

		siRNA screen			CRISPR Screen		
	Gene	Median Seed Corrected Z-Score	P-value	Rank	log2FC	P-value	Rank
UPF proteins	UPF1	1.76	3.05E-03	62	1.96	2.21E-04	6
	UPF2	0.98	>0.05	193	4.07	2.26E-03	15
	UPF3B	0.72	1.15E-02	470	0.15	>0.1	1828
SMG proteins	SMG1	7.60	2.41E-03	1	na	na	na
	SMG5	2.25	3.20E-03	47	4.03	< 10E-06	1
	SMG6	4.75	2.47E-03	14	3.86	< 10E-06	2
	SMG7	2.14	2.77E-03	51	6.32	< 10E-06	3
	SMG8	0.44	2.28E-03	1469	na	na	na
	SMG9	0.17	>0.1	3859	na	na	na
core EJC	EIF4A3	6.90	2.41E-03	3	na	na	na
	RBM8A	7.04	2.41E-03	2	na	na	na
	MAGOH	5.65	2.43E-03	8	na	na	na
	CASC3	3.92	2.57E-03	19	1.28	4.13E-01	120
EJC assembly & associated	CWC22	1.07	1.22E-02	150	0.60	>0.1	1450
	AQR	6.46	2.42E-03	6	na	na	na
	ACIN1	0	>0.1	13890	1.33	>0.05	412
	RNPS1	-0.70	>0.1	20388	na	na	na
other	NBAS	0.26	>0.1	2955	na	na	na
	PNRC2	0.52	>0.05	1074	na	na	na
	DHX34	0	>0.1	6499	-0.37	>0.1	3715

= p-value < 0.05

na = no sgRNAs sequenced

Figure 1—figure supplement 2. Comparison of siRNA and CRISPR screens. (**A**) Venn diagram of genes identified as top hits in the RNAi screen and a published CRISPR screen for NMD factors. Shown are genes with positive seed-corrected Z-scores (siRNA) or fold change (CRISPR, with gene-level

Figure 1—figure supplement 2 continued on next page

Figure 1—figure supplement 2 continued

analysis using MAGeCK software) and *P*-values less than 0.05. Genes identified in both screens are listed, with known NMD factors highlighted in red. (**B**) Recovery of proteins previously implicated in NMD in the siRNA and CRISPR screens. Green indicates p-values less than 0.05. Rank Z-score (RNAi) or rank MAGeCK score (CRISPR) are shown. For CRISPR data, 'na' indicates that no sgRNA sequences were identified in the input pool.

DOI: https://doi.org/10.7554/eLife.33178.005

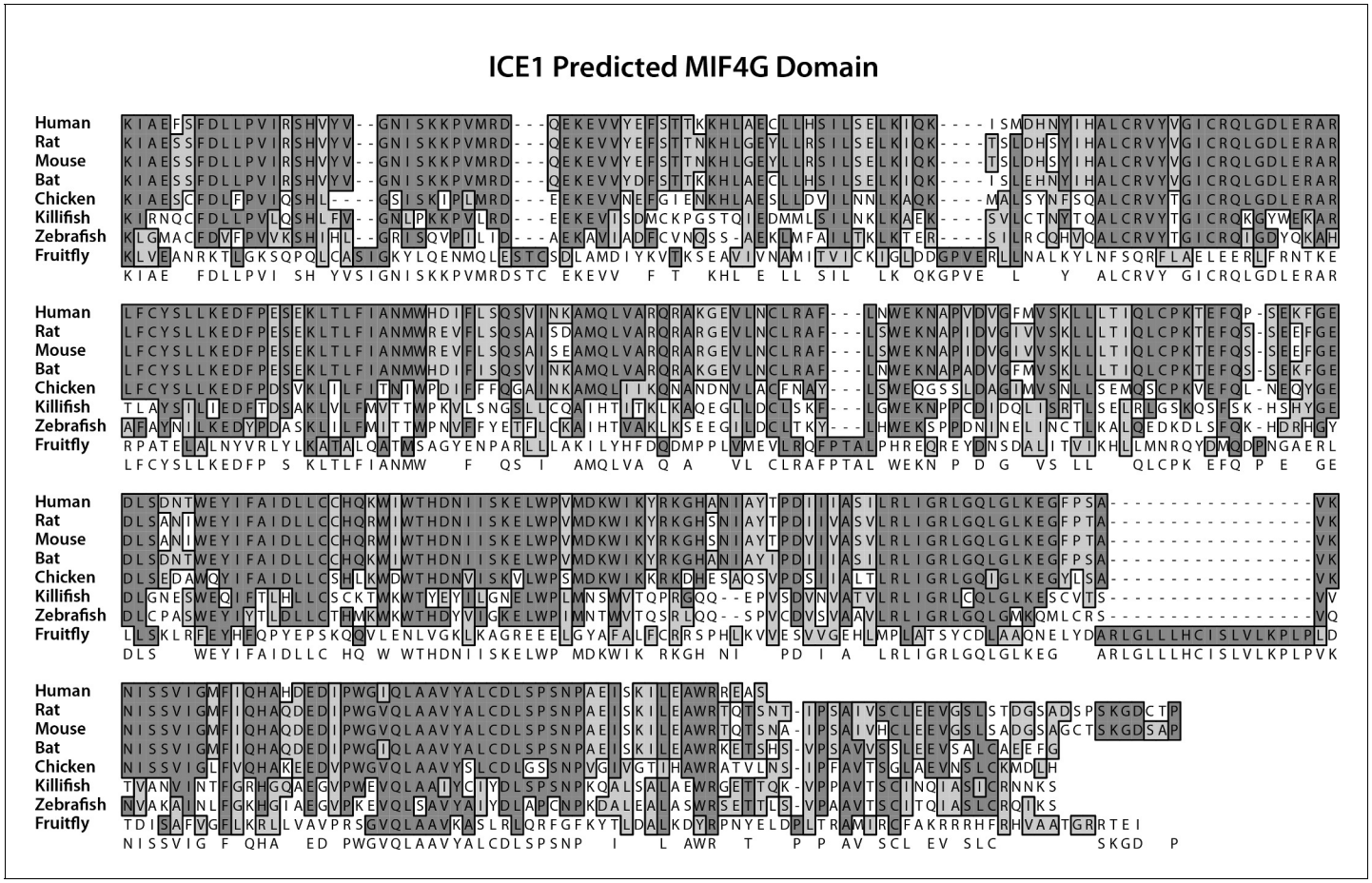

Figure 1—figure supplement 3. Phylogenetic alignment of the predicted ICE1 C-terminal MIF4G domain. T-Coffee multiple sequence alignment of the ICE C-terminus from human (*H. sapiens*), rat (*R. norvegicus*), platypus (*O. anatinus*), chicken (*G. gallus*), zebrafish (*D. rerio*), coelacanth (*L. chalumnae*), and frog (*X. tropicalis*). Absolutely conserved residues are shaded in dark grey, while functionally conserved residues are shaded in light grey. Similarity scores with Human ICE1 are 90.9% (Rn), 85.8% (Oa), 75.4% (Gg), 67.2% (Dr), 77.7% (Lc), and 76.3 (Xt).

DOI: https://doi.org/10.7554/eLife.33178.006

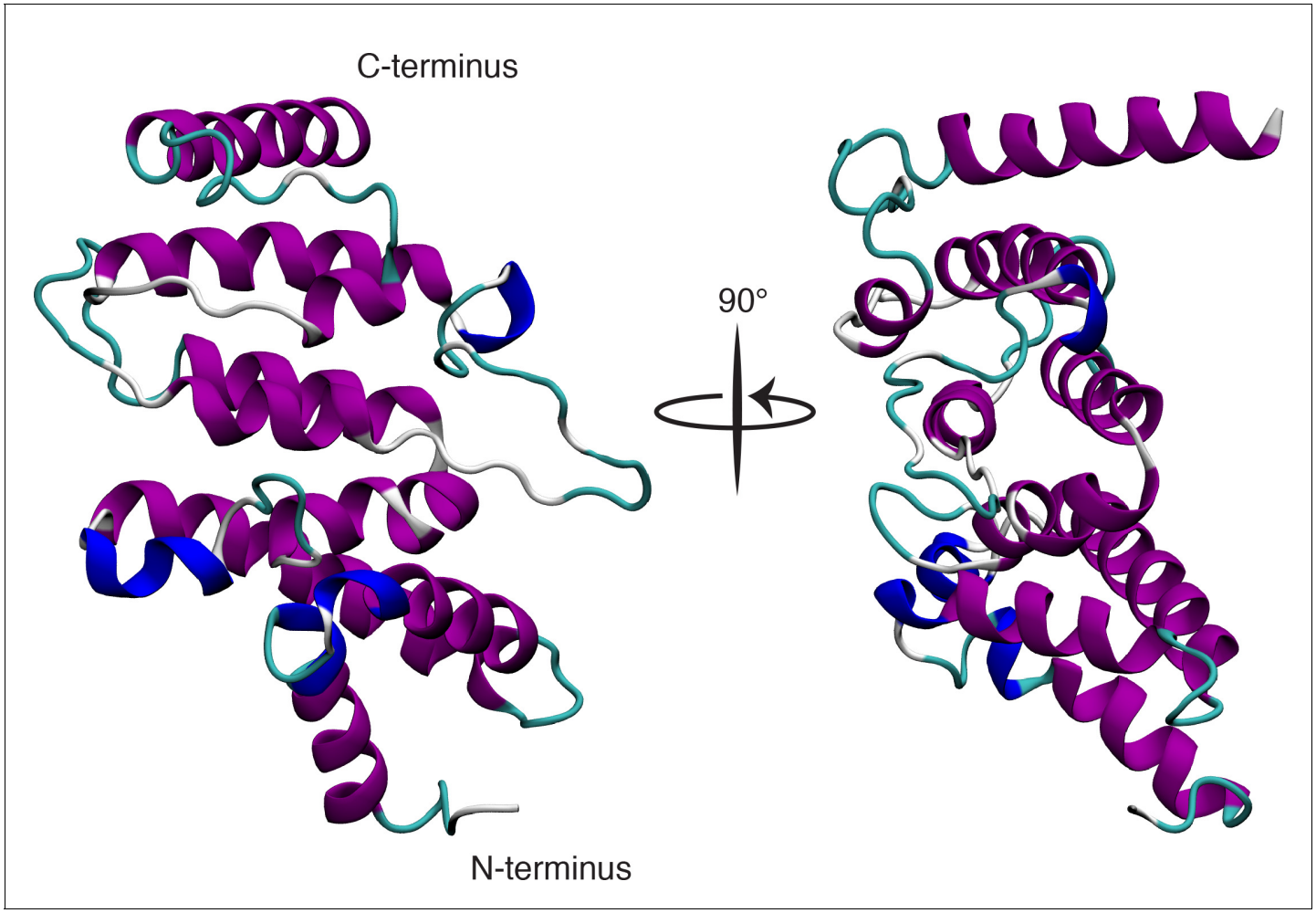

Figure 1—figure supplement 4. Predicted MIF4G domain of ICE1 modeled on third MIF4G domain of UPF2. Protein Homology/analogY Recognition Engine V 2.0 (PHYRE[2]) software predicted a putative MIF4G domain in the C-terminus of ICE1 based on the known structure of the third MIF4G domain of UPF2 with 94% confidence.

DOI: https://doi.org/10.7554/eLife.33178.007

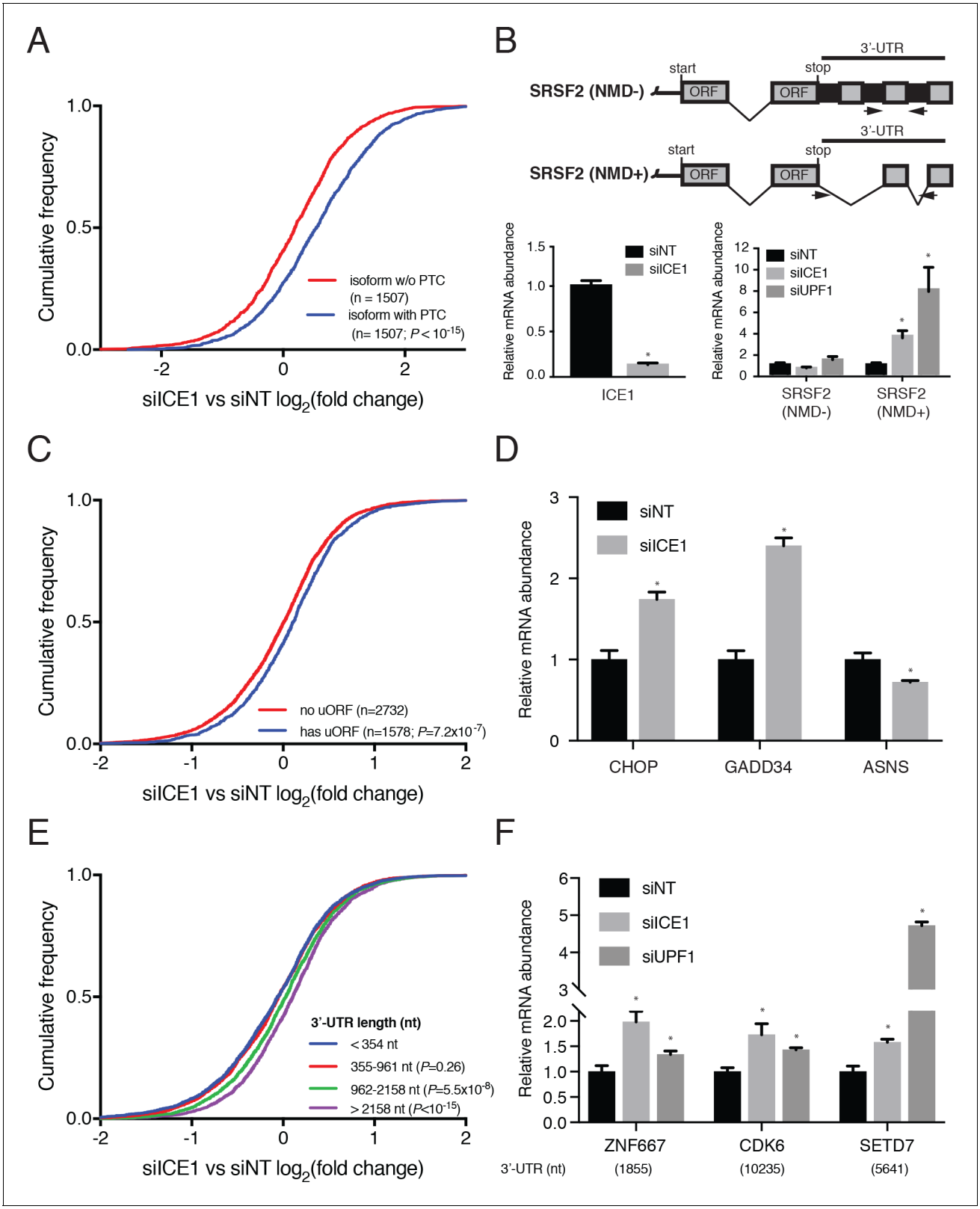

Figure 2. ICE1 depletion results in increased abundance of NMD substrates. (**A**) CDF plot of the effect of ICE1 depletion on mRNA isoforms containing and lacking PTCs as defined using the 50 nt rule. Only genes with detectable expression of both isoform types were considered. Statistical significance was determined by K-S test. (**B**) (Top) Schematic illustrating SRSF2 splicing isoforms with differential sensitivity to the NMD pathway. (Bottom) RT-qPCR

Figure 2 continued on next page

Figure 2 continued

analysis of NMD-insensitive and -sensitive SRSF2 transcript isoforms during ICE1 and UPF1 depletion. ICE1 knockdown efficiency shown on the left is for the cDNA libraries used in ***Figure 2B,D and F***. (**C**) CDF plot of the effect of ICE1 depletion on expression of mRNAs previously determined to contain or lack actively translated uORFs. Statistical significance was determined by K-S test. (**D**) RT-qPCR analysis of uORF-containing mRNAs CHOP and GADD34 during ICE1 depletion. (**E**) Response to ICE1 depletion among genes (n = 11057) divided into quartiles according to the 3'UTR length of the most highly expressed isoform detected in Kallisto analyses. Statistical significance was determined by K-S test. (**F**) RT-qPCR analysis of NMD substrates with long 3'-UTRs during ICE1 and UPF1 depletion. 3'-UTR lengths are provided in nucleotides (nt) beneath the X-axis. Data represent mean values with error bars illustrating standard deviation. Asterisks indicate statistical significance (n = 3, Student's t-test, $p<0.05$) between non-targeting and gene-specific siRNA knockdown values.

DOI: https://doi.org/10.7554/eLife.33178.009

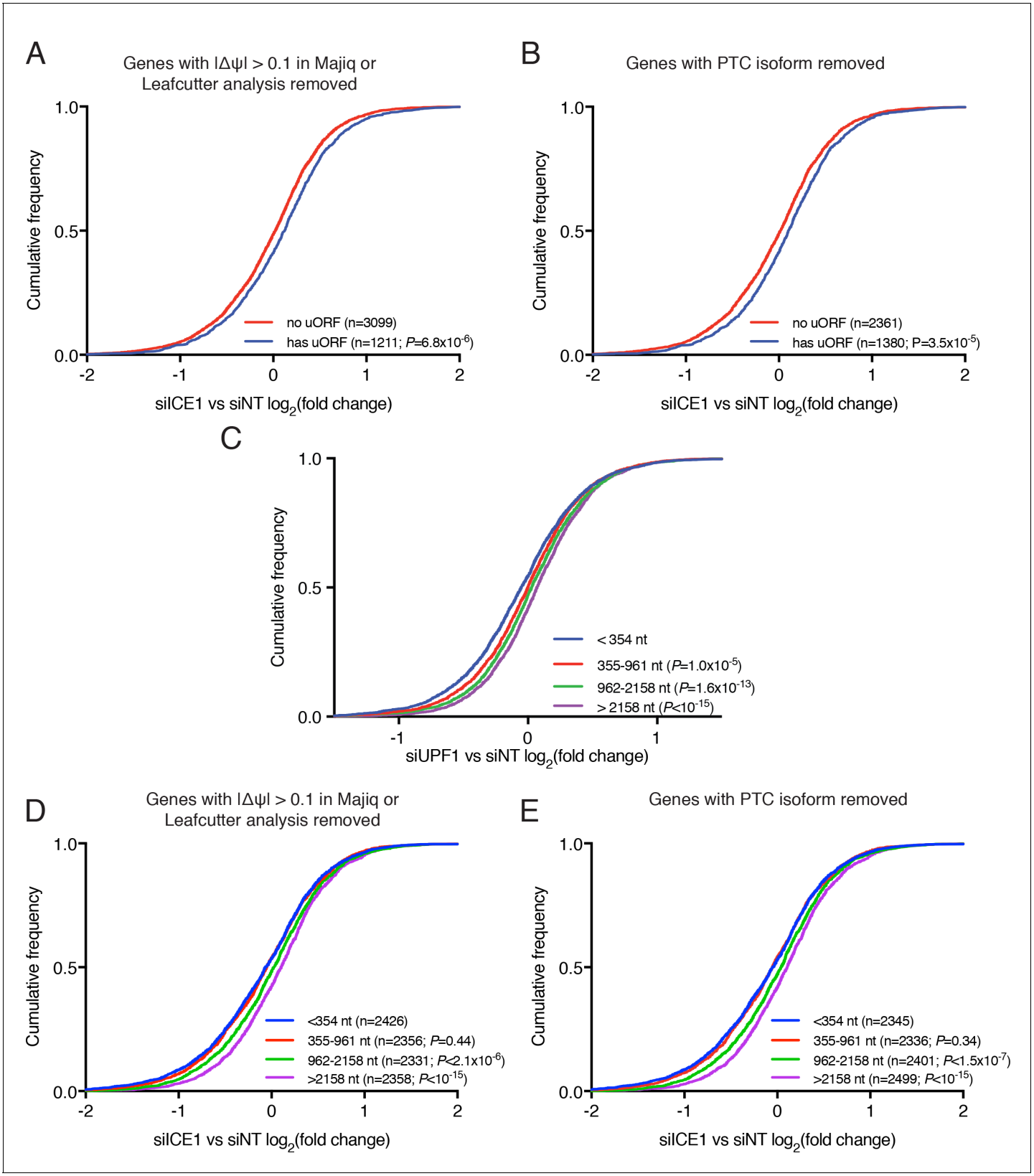

Figure 2—figure supplement 1. Analysis of the effect of ICE1 and UPF1 depletion on mRNAs with uORFs and long 3'UTRs. (**A**) CDF plot of the response to ICE1 knockdown among genes with or without validated uORFs, as in ***Figure 2C***. Genes with evidence of alternative splicing in either Majiq or Leafcutter analyses were removed. (**B**) CDF plot as in A, except that genes with PTC isoforms analyzed in ***Figure 2A*** were removed. (**C**) CDF

Figure 2—figure supplement 1 continued on next page

Figure 2—figure supplement 1 continued

plot illustrating the response to UPF1 knockdown among genes divided into quartiles according to the 3'UTR length of the most highly expressed isoform in Kallisto analyses. p-Values are derived from K-S tests relative to the shortest class of 3'UTR. (**D**) CDF plot as in A, except that genes were categorized according to 3'UTR length as in ***Figure 2E***. (**E**) CDF plot as in B, except that genes were categorized according to 3'UTR length as in ***Figure 2E***. Statistical significance was determined by K-S test in all panels.

DOI: https://doi.org/10.7554/eLife.33178.010

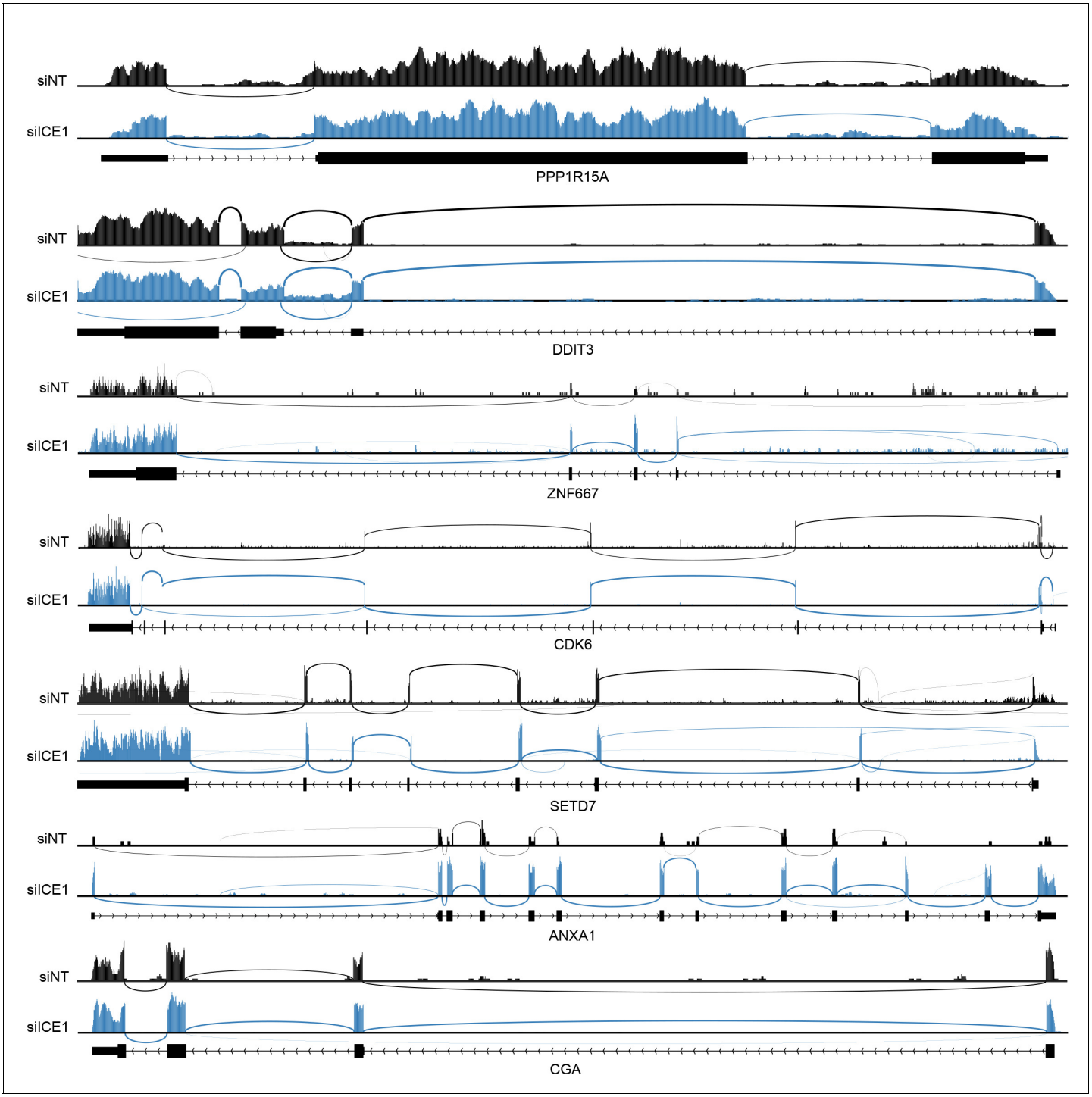

Figure 2—figure supplement 2. RNAseq traces for NMD targets during control and ICE1 depletion. Representative RNAseq histograms from cells treated with non-silencing (siNT) or anti-ICE1 (siICE1) siRNAs for the indicated genes are shown. Reads were mapped with HISAT2 as described in Materials and methods. Sashimi plots were generated using Integrated Genomics Viewer Software. Each sample was auto-scaled according to the highest peak within the window shown.

DOI: https://doi.org/10.7554/eLife.33178.011

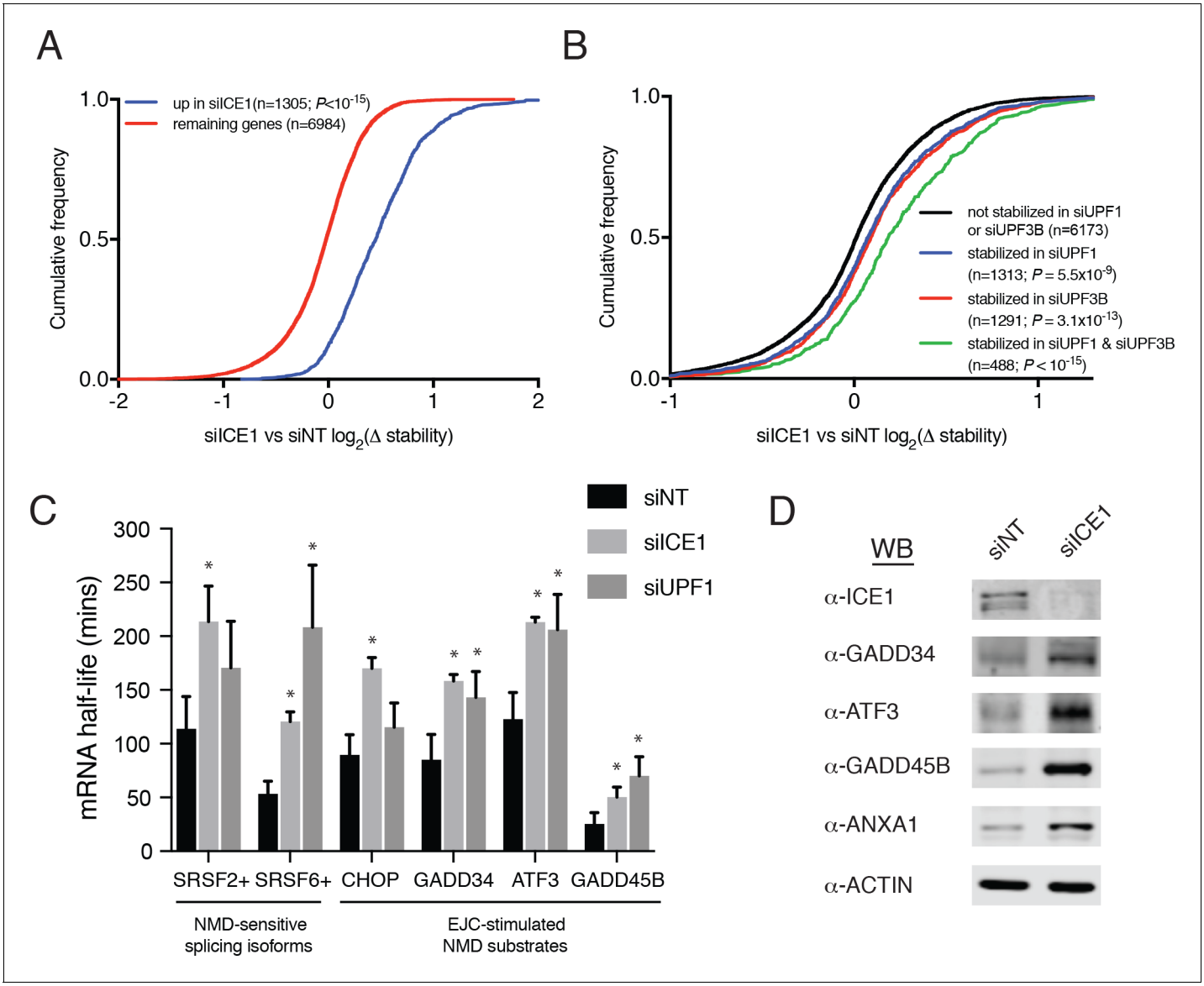

Figure 3. ICE1 depletion causes stabilization and translation of NMD target mRNAs. (**A**) CDF plot of relative mRNA stability as determined by REMBRANDTS analysis of RNAseq following siICE or siNT treatment, categorized according to the change in steady-state mRNA levels upon siICE1 treatment. Transcripts were classified as increased in siICE1 if they exhibited a log2(FC) >0.5 and a Sleuth q-value <0.05. Statistical significance was determined by K-S test. (**B**) CDF plot as in (**A**), with genes categorized according to their relative stability changes in response to UPF1 or UPF3B knockdown. Transcripts with log2(Δstablity)>0.2 and p-value<0.05 were classified as stabilized. Statistical significance was determined by K-S test. (**C**) Gene-specific mRNA half-lives during siRNA depletion as determined by 5-EU metabolic labeling. Bars represent mean half-life values from three biological replicates, error bars indicate standard deviation, and asterisks mark significant differences between treatments (Student's t-test; p<0.05). (**D**) Western blot of protein levels from HEK-293 lysates depleted of ICE1 (siICE1) or a non-targeting control (siNT).

DOI: https://doi.org/10.7554/eLife.33178.012

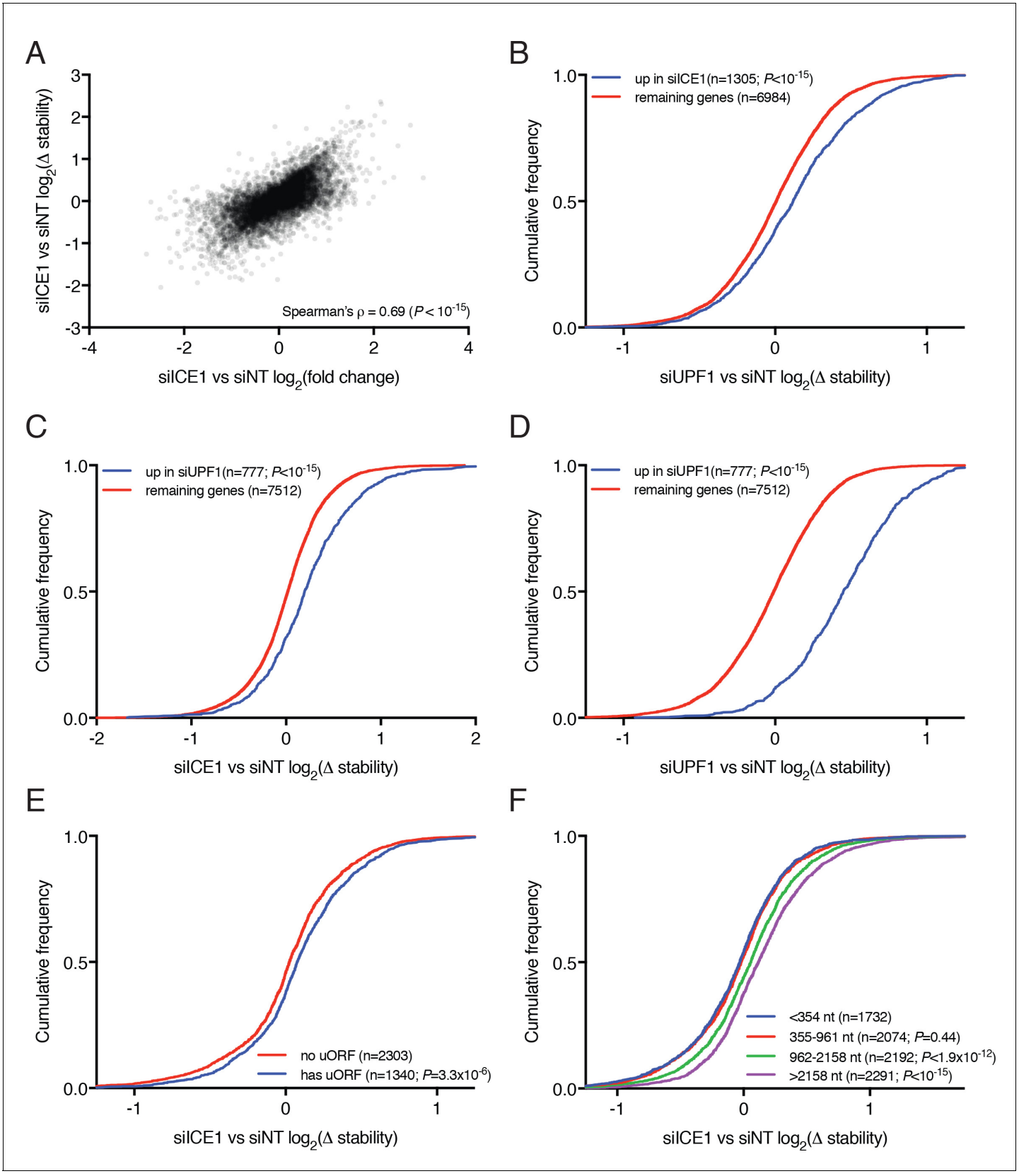

Figure 3—figure supplement 1. Analysis of mRNA stability changes upon UPF1 and ICE1 depletion. (**A**) Scatterplot of changes in mRNA relative stability as determined by REMBRANDTS and relative abundance as determined by Kallisto, comparing siICE1 to siNT treatment. (**B**) CDF plot of

Figure 3—figure supplement 1 continued on next page

Figure 3—figure supplement 1 continued

relative mRNA stability as determined by REMBRANDTS analysis of RNAseq following siUPF1 or siNT treatment, categorized according to the change in steady-state mRNA levels upon siICE1 treatment. Transcripts were classified as increased in siICE1 if they exhibited a log2(FC) >0.5 and a Sleuth q-value <0.05. Statistical significance was determined by K-S test. (**C**) CDF plot as in B, with relative stability measurements of siICE1 vs. siNT treatment, categorized by changes in steady-state mRNA levels in siUPF1 treatment. (**D**) CDF plot as in C, except illustrating relative stability measurements of siUPF1 vs. siNT treatment. (**E**) CDF plot of changes in relative mRNA stability upon ICE1 depletion, with genes categorized by the presence or absence of a validated uORF as in ***Figure 2C***. Statistical significance was determined by K-S test. (**F**) CDF plot as in E, with genes categorized by 3'UTR length as in ***Figure 2E***.

DOI: https://doi.org/10.7554/eLife.33178.013

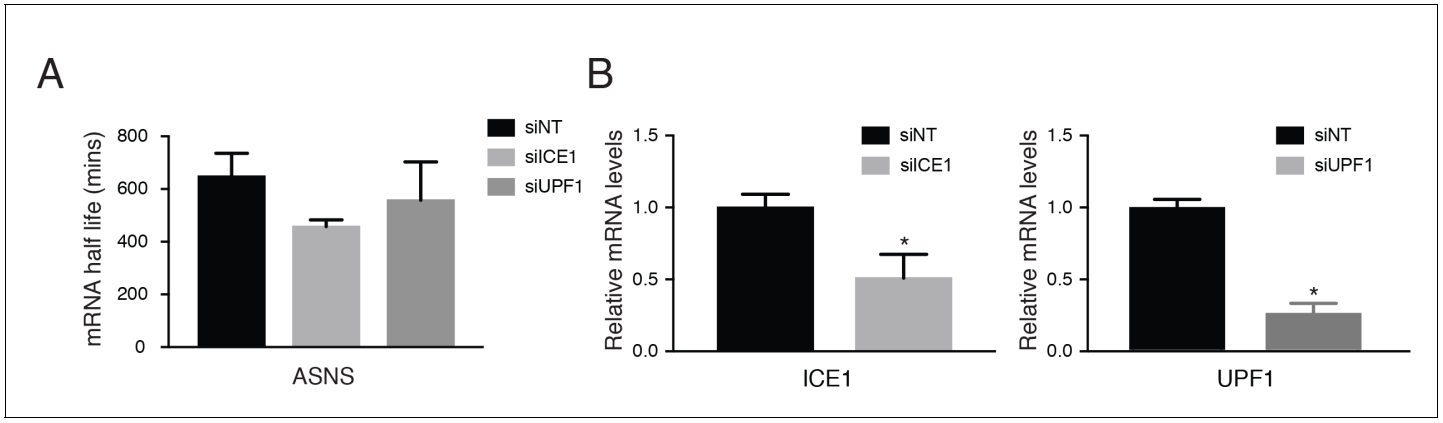

Figure 3—figure supplement 2. ICE1 and UPF1 depletion controls and knockdown efficiencies in metabolic labeling studies. (**A**) mRNA half-life measurements of ASNS during ICE1 and UPF1 gene depletion. ASNS serves as a control member of the ISR pathway that is not subject to EJC-enhanced NMD. (**B**) qPCR illustrating mRNA values of ICE1 and UPF1 levels from 'total' cDNA libraries. Bars represent mean mRNA abundance, error bars indicate standard deviation, and asterisks denote statistical significance as compared to the non-targeting control (n = 3, Student's t-test; $p<0.05$).
DOI: https://doi.org/10.7554/eLife.33178.014

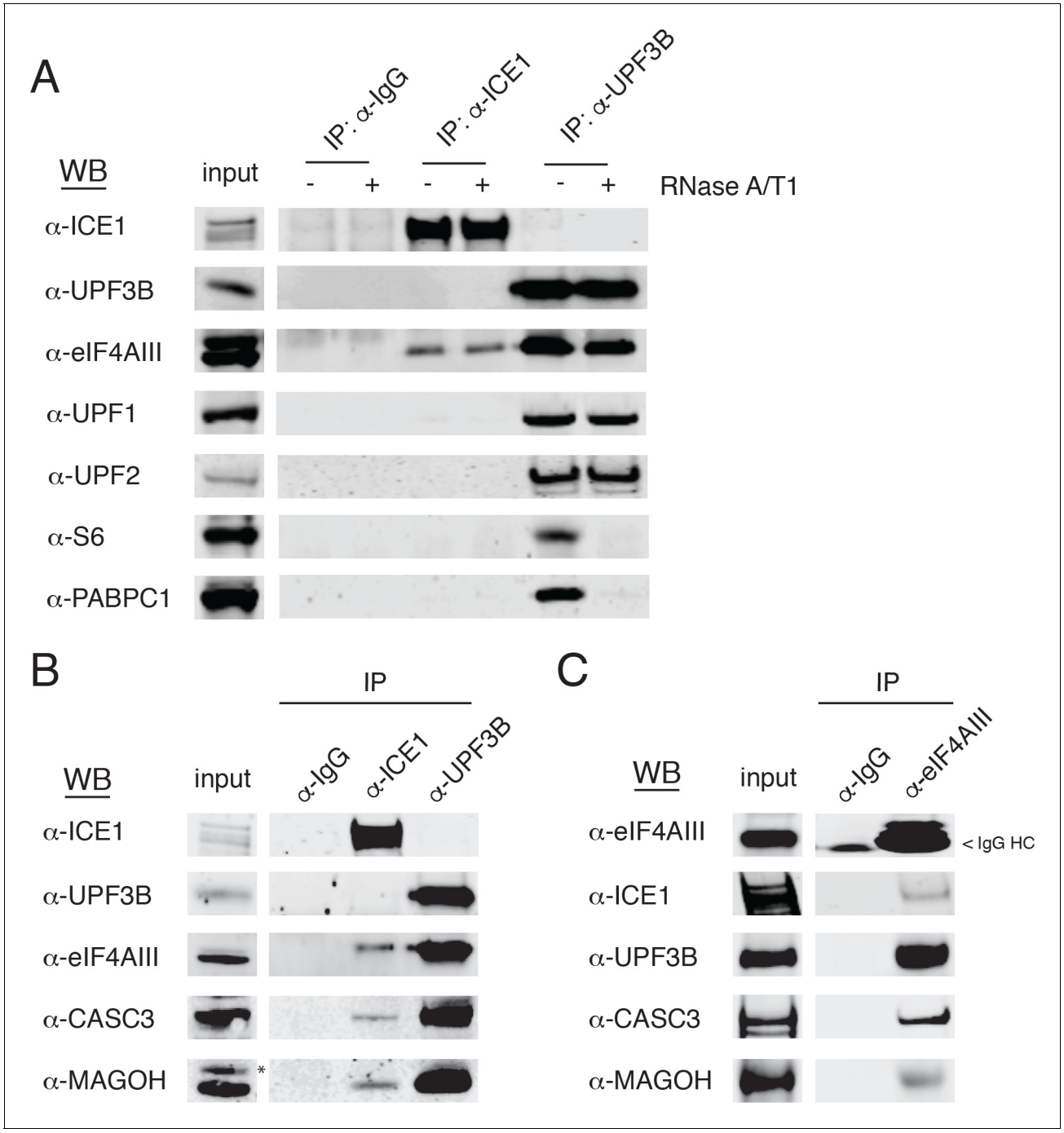

Figure 4. ICE1 co-immunopurifies with the core EJC in HEK-293 cells. (**A**) Western blot showing lysates subject to co-immunoprecipitation with control IgG, ICE1 or UPF3B antibodies. Lysates were treated with RNase A/T1 cocktail during the copurification (+) or untreated (-), and antibodies against the indicated proteins were used for detection. (**B**) Western blot of cell lysates subject to co-immunoprecipitation with control IgG, ICE1 or UPF3B antibodies. Antibodies against the core EJC members used for detection are indicated at the left, and asterisk indicates non-specific band. (**C**) Western blot of lysates subject to co-immunoprecipitation with control IgG or monoclonal eIF4AIII antibody. Antibodies used for detection of the core and peripheral EJC components are indicated. Input lanes represent 3% of the total immunoprecipitated material.

DOI: https://doi.org/10.7554/eLife.33178.015

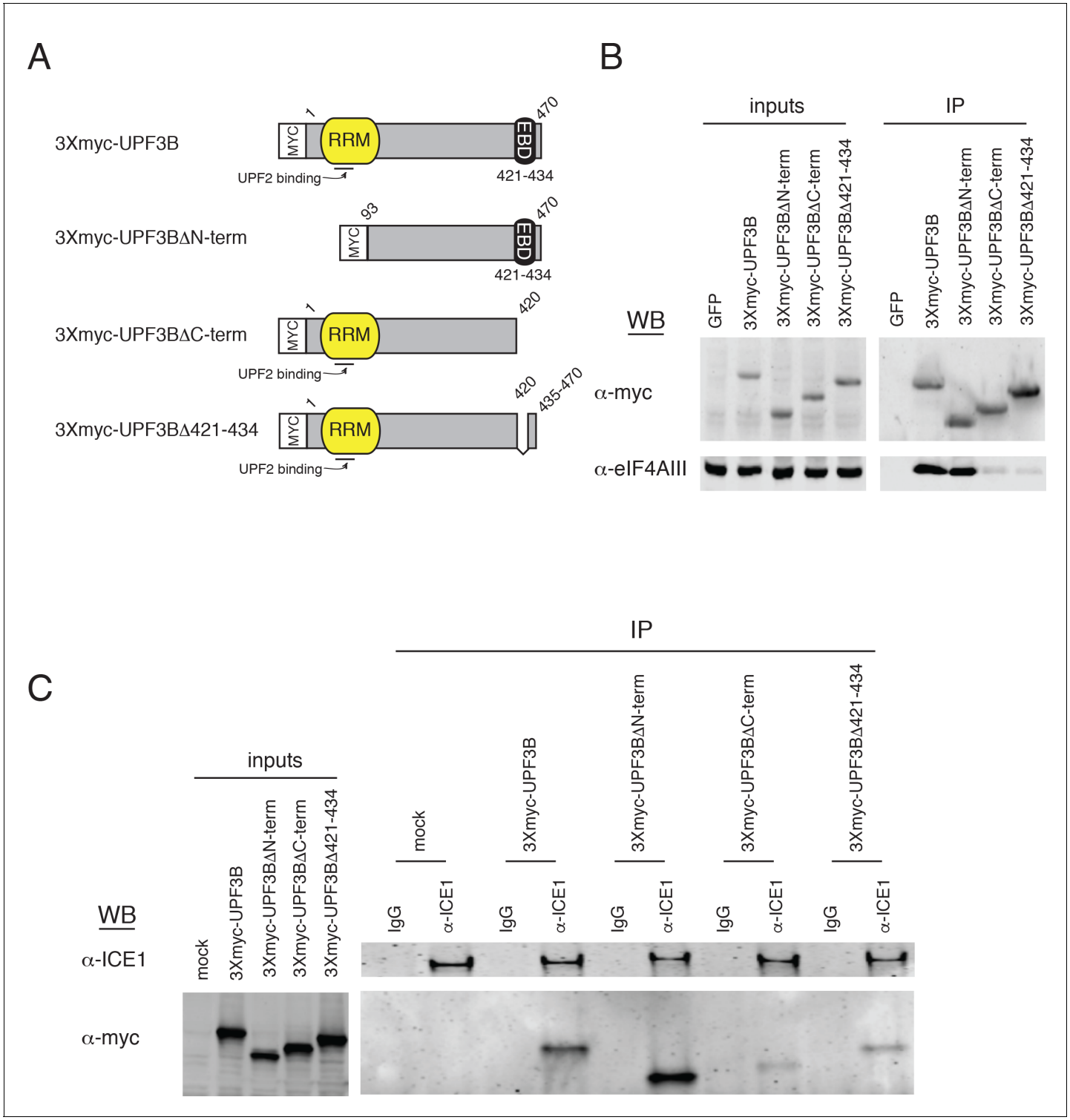

Figure 4—figure supplement 1. ICE1 copurifies with overexpressed UPF3B in an EJC-dependent manner. (**A**) Schematic of reporter constructs expressed in HEK-293 cells for immunoprecipitation studies. RRM = RNA recognition motif; EBD = exon junction binding domain. (**B**) Immunoblot of HEK-293 cell lysates transiently overexpressing 3Xmyc-tagged version of the reporters in panel A subjected to immunoprecipitation with anti-myc antibody. Antibodies for probing are indicated on the left, and input lanes represent 3% of the total immunoprecipitated material. (**C**) Immunoblot of HEK-293 cell lysates transiently overexpressing 3Xmyc-tagged versions of the reporters in panel A subjected to immunoprecipitation with an anti-ICE1 antibody. Antibodies for probing are indicated on the left, and input lanes represent 3% of the total immunoprecipitated material.

DOI: https://doi.org/10.7554/eLife.33178.016

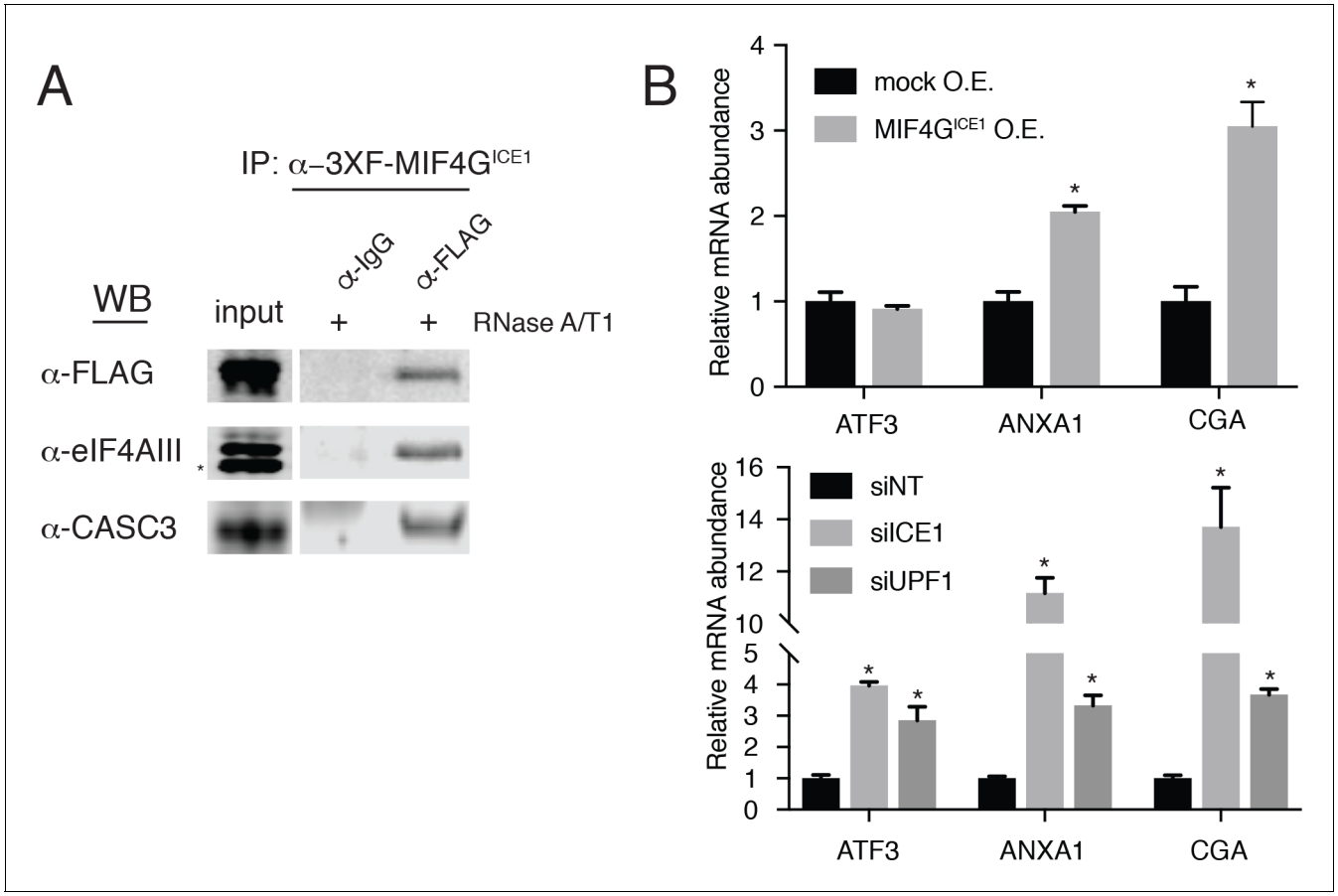

Figure 5. The putative MIF4G domain of ICE1 is sufficient to interact with eIF4AIII. (**A**) Western blot of cell lysates stably expressing mock or 3XFLAG-tagged putative ICE1 MIF4G domain (3XFLAG-MIF4G^{ICE1}) were subjected to coimmunoprecipitation with a FLAG antibody. Lysates were treated with RNase A/T1 cocktail during the copurification (+), and antibodies used for detection are indicated at the left. Input lanes represent 3% of the total immunoprecipitated material. (**B**) (Top) RT-qPCR analysis of the NMD targets ATF3, ANXA1 and CGA in HEK-293 cells expressing a mock plasmid or vector expressing 3XFLAG-tagged putative ICE1 MIF4G domain. (Bottom) RT-qPCR analysis of ATF3, ANXA1 and CGA levels in cells depleted of ICE1 or UPF1. ICE1 knockdown efficiency is represented in ***Figure 2B***. Data represent mean values with error bars illustrating standard deviation. Asterisks indicate statistical significance between control and 'treatment' values for each experiment (n = 3, Student's t-test, $p<0.05$).

DOI: https://doi.org/10.7554/eLife.33178.017

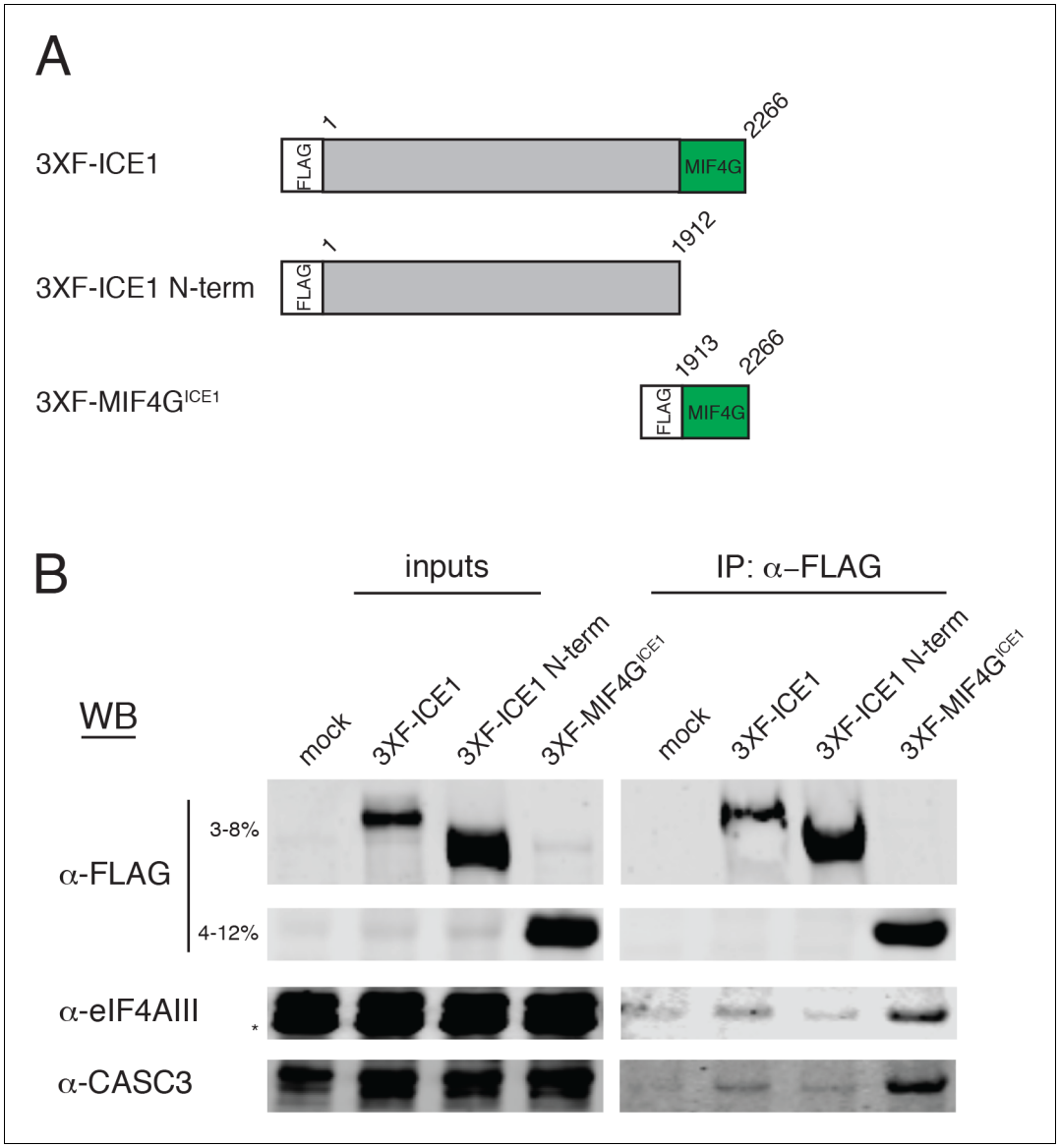

Figure 5—figure supplement 1. The C-terminus of ICE1 is sufficient to recover eIF4AIII. (**A**) Schematic of reporter constructs expressed in HEK-293 cells for immunoprecipitation studies. MIF4G = middle domain of eukaryotic initiation factor 4G. (**B**) Immunoblot of HEK-293 cell lysates transiently overexpressing 3XFLAG-tagged version of the reporters in panel A subjected to immunoprecipitation with anti-FLAG antibody. Antibodies for probing are indicated on the left, and input lanes represent 3% of the total immunoprecipitated material.

DOI: https://doi.org/10.7554/eLife.33178.018

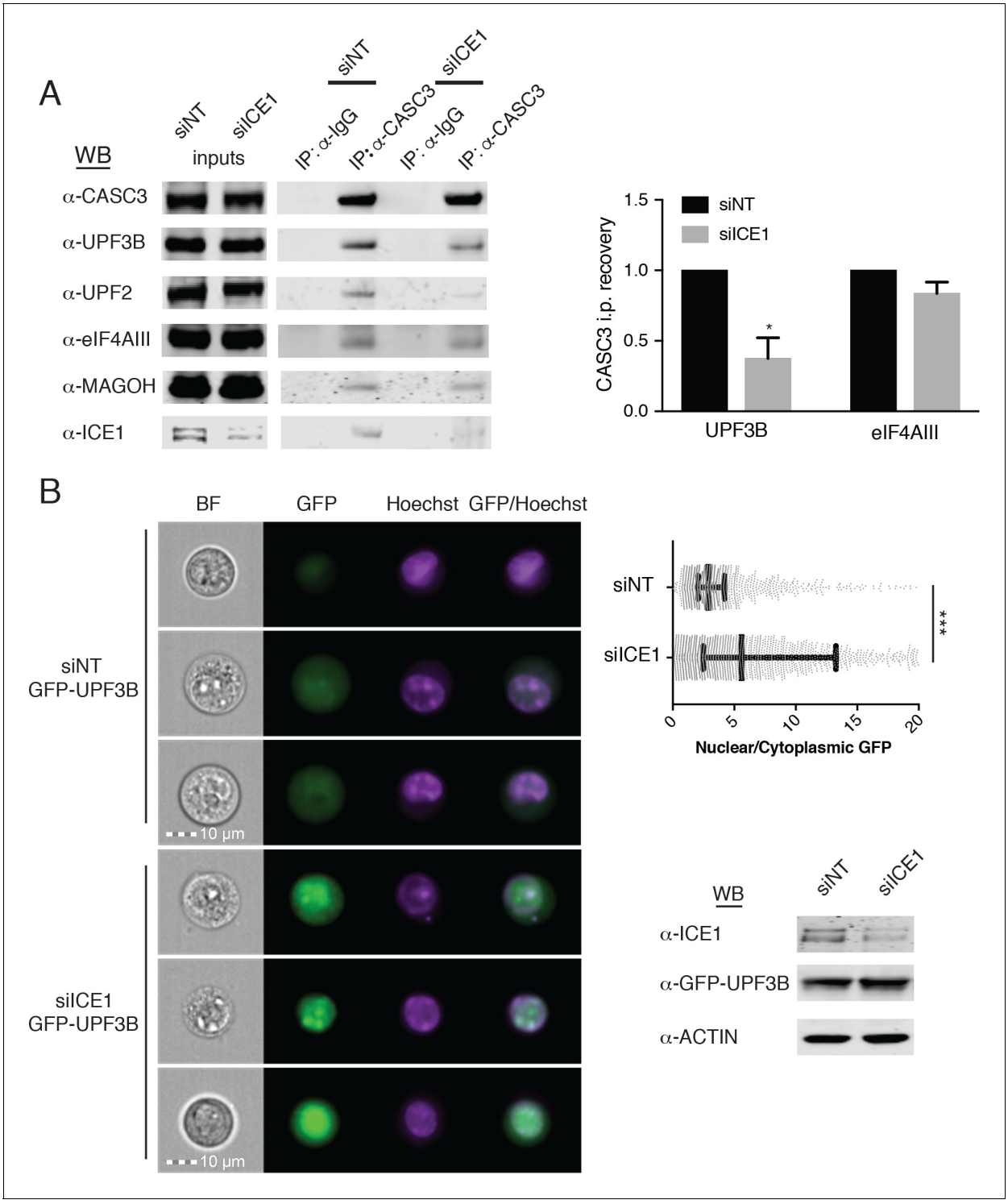

Figure 6. ICE1 is required for UPF3B association with the EJC. (**A**) (Left) Western blot of cell lysates depleted with negative control or ICE1 siRNAs were subjected to co-immunoprecipitation with IgG or CASC3 antibodies. Antibodies against UPF and EJC proteins were used for detection, as indicated on the left. (Right) Quantification of three independent experiments showing densitometry values of UPF3B or eIF4AIII recovery during CASC3 i.p. with or without ICE1 depletion. Error bars represent standard deviation, and the asterisk indicates statistical significance compared to control (Student's t-test, $p<0.05$). (**B**) (Left) Imaging flow cytometry of 293 cells stably expressing GFP-UPF3B fusion protein during ICE1 or control depletion. Images presented represent unbiased collection events generated by IDEAS software from each treatment group's median bin. (Top right) Quantification of nuclear/cytosolic GFP-UPF3B fusion protein ratios during ICE1 depletion or control. Bars represent 25th, 50th, and 75th quartile for each treatment group, and

Figure 6 continued on next page

Figure 6 continued

asterisks indicate statistical significance (n = 1588 (siNT); n = 2167 (siICE1); Mann Whitney test, p<10–15). (Bottom right) Western blot of total GFP-UPF3B protein levels during ICE1 depletion.

DOI: https://doi.org/10.7554/eLife.33178.019

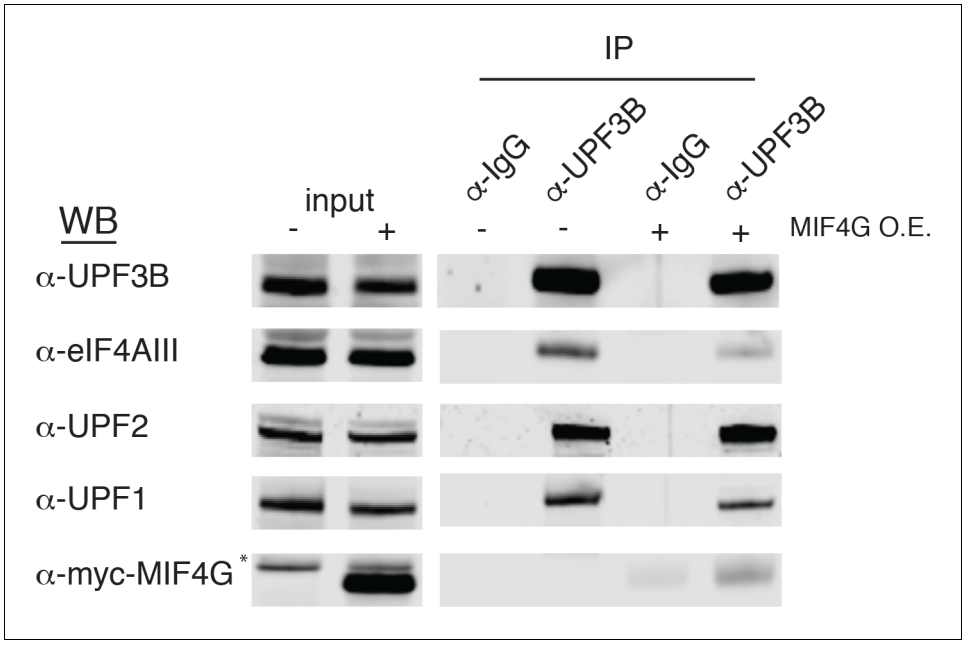

Figure 6—figure supplement 1. Overexpression of the ICE1 MIF4G domain disrupts interaction of UPF3B with eIF4AIII. Western blot of HEK-293 cell lysates transiently overexpressing 3Xmyc-ICE1 MIF4G (a.a. 1921–2266) subjected to immunoprecipitation with an anti-UPF3B antibody. Antibodies for probing are indicated on the left, and input lanes represent 3% of the total immunoprecipitated material.

DOI: https://doi.org/10.7554/eLife.33178.020

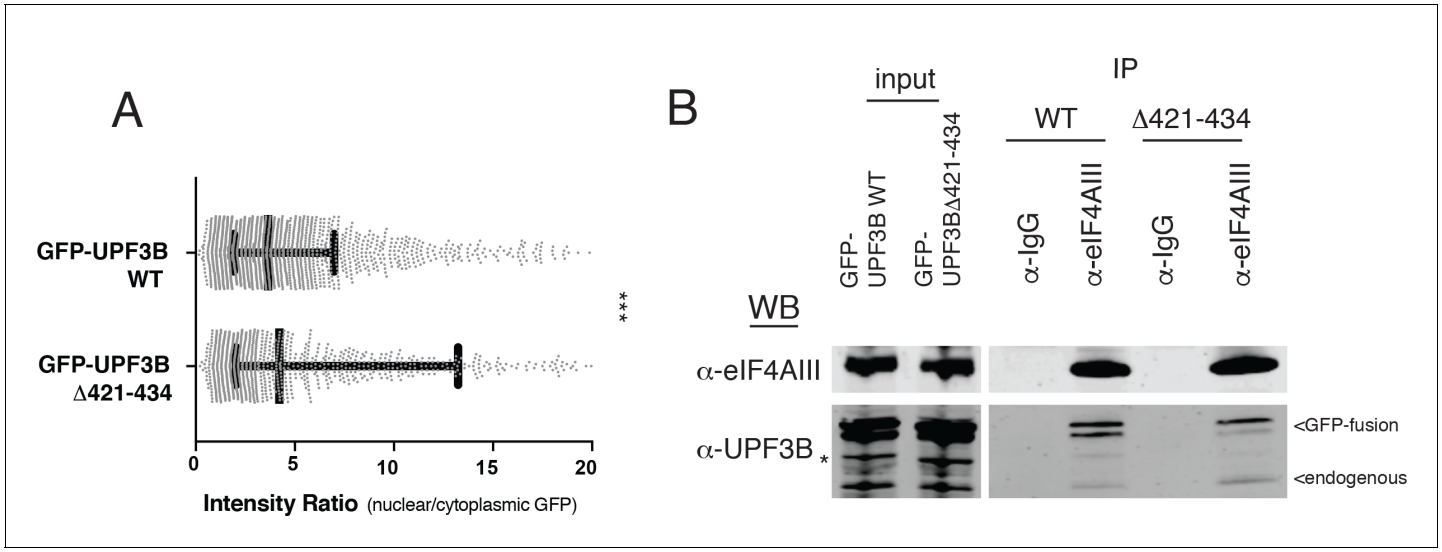

Figure 6—figure supplement 2. An EJC-binding mutant of GFP-UPF3B is enriched in the nucleus. (**A**) Imaging flow cytometry comparing nuclear/cytoplasmic eGFP ratios between UPF3B WT and UPF3B lacking amino acid residues 421–434. Whiskers represent the 25th, 50th, and 75th percentiles, while asterisks indicate statistical significance between groups (n = 1980; n = 1234; Mann Whitney test, p<0.0001). (**B**) Immunoblot of lysates from stable cell lines expressing GFP-UPF3B or GFP-UPF3BΔ421–434 (deletion of EJC-interacting a.a. 412–434) subjected to immunoprecipitation with anti-eIF4AIII antibody and probed with the antibodies indicated on the left. Input lanes represent 3% of the total immunoprecipitated material, and asterisk denotes non-specific band.

DOI: https://doi.org/10.7554/eLife.33178.021

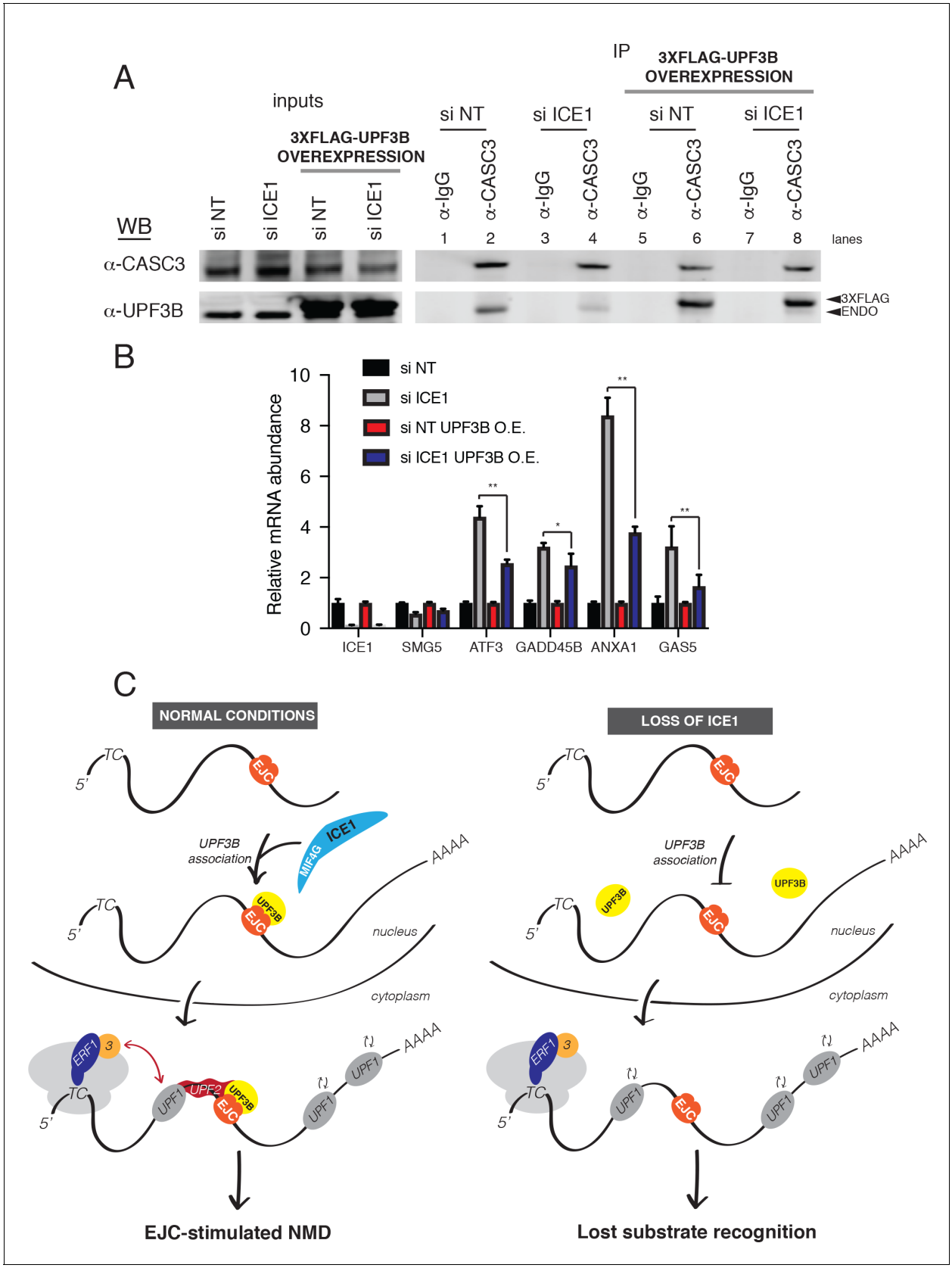

Figure 7. UPF3B overexpression ameliorates NMD defect during ICE1 depletion. (**A**) Western blot of cell lysates engineered to stably overexpress 3XFLAG-UPF3B or parental vector treated with ICE1 or non-targeting control siRNAs. Co-immunoprecipitation of the EJC was performed using anti-

Figure 7 continued on next page

Figure 7 continued

CASC3 antibodies. Input lanes represent 3% of the total immunoprecipitated material. (**B**) RT-qPCR analysis of EJC-stimulated targets in parental or UPF3B overexpression cell lines depleted of ICE1 or a non-targeting control. Asterisks indicate statistical significance in fold change between parental and UPF3B overexpression lines during ICE1 depletion (n = 3, Student's t-test, *p<0.05; **p<0.01). (**C**) Model illustrating the requirement of ICE1 to facilitate UPF3B association with the EJC and subsequently target EJC-stimulated NMD substrates for decay.

DOI: https://doi.org/10.7554/eLife.33178.022